Available online at www.sciencedirect.com
SCIENCE DIRECT
Bioorganic & Medicinal Chemistry
ELSEVIER
Bioorganic & Medicinal Chemistry 14 (2006) 1378–1390

Discovery of potent and selective PARP-1 and PARP-2 inhibitors: SBDD analysis via a combination of X-ray structural study and homology modeling

Junya Ishida,[a] Hirofumi Yamamoto,[a] Yoshiyuki Kido,[a] Kazunori Kamijo,[a] Kenji Murano,[a] Hiroshi Miyake,[a] Mitsuru Ohkubo,[b] Takayoshi Kinoshita,[b] Masaichi Warizaya,[b] Akinori Iwashita,[c] Kayoko Mihara,[c] Nobuya Matsuoka[c] and Kouji Hattori[a,*]

[a]*Medicinal Chemistry Research Laboratories, Fujisawa Pharmaceutical Co. Ltd, 2-1-6 Kashima, Yodogawa-ku, Osaka 532-8514, Japan*
[b]*Exploratory Research Laboratories, Fujisawa Pharmaceutical Co. Ltd, 5-2-3 Tokodai, Tsukuba, Ibaraki 300-2698, Japan*
[c]*Medicinal Biology Research Laboratories, Fujisawa Pharmaceutical Co. Ltd, 2-1-6 Kashima, Yodogawa-ku, Osaka 532-8514, Japan*

Received 16 May 2005; revised 26 September 2005; accepted 27 September 2005
Available online 8 November 2005

Abstract—We disclose herein our efforts aimed at discovery of selective PARP-1 and PARP-2 inhibitors. We have recently discovered several novel classes of quinazolinones, quinazolidinones, and quinoxalines as potent PARP-1 inhibitors, which may represent attractive therapeutic candidates. In PARP enzyme assays using recombinant PARP-1 and PARP-2, the quinazolinone derivatives displayed relatively high selectivity for PARP-1 and quinoxaline derivatives showed superior selectivity for PARP-2, and the quinazolidinone derivatives did not have selectivity for PARP-1/2. Structure-based drug design analysis via a combination of X-ray structural study utilizing the complexes of inhibitors and human PARP-1 catalytic domain, and homology modeling using murine PARP-2 suggested distinct interactions of inhibitors with PARP-1 and PARP-2. These findings provide a new structural framework for the design of selective inhibitors for PARP-1 and PARP-2.

1. Introduction

Poly(ADP-ribose) polymerase (PARP) is an abundant nuclear enzyme in eukaryotic cells that has been implicated to become activated in response to DNA damage. Activated PARP catalyzes the transfer of ADP-ribose units from nicotinamide adenine dinucleotide (NAD^+) to nuclear acceptor proteins such as histones, topoisomerases, DNA polymerases, DNA ligases, and PARP itself. Excessive activation of PARP consumes NAD^+ and consequently ATP, culminating in cell dysfunction or necrosis. Furthermore, PARP has also been implicated in a caspase-independent apoptosis pathway mediated by apoptosis-inducing factor.[1] PARP inhibitors provided remarkable protection from tissue damage in various forms of reperfusion injury, inflammation, and neurotoxicity in animal models.[2] Thus, inhibition of PARP by pharmacological agents could be useful in the treatment of inflammatory disease, neurodegenerative disease, and several other diseases involved in PARP activation.

Characterized family members of PARP currently include the proteins PARP-1, PARP-2, PARP-3, Tankyrase-1, Tankyrase-2, TiPARP, and vPARP. Although PARP-1 has been believed to be responsible for all the DNA-damage-dependent poly(ADP-ribose) (PAR) synthesis in mammalian cells, a novel DNA-damage-dependent PARP-2 was subsequently discovered as a result of the presence of residual DNA-dependent PARP activity

Keywords: PARP-1, poly(ADP-ribose)polymerase-1; PARP-2, poly (ADP-ribose) polymerase-2 (PARP-2); NAD^+, nicotinamide adenine dinucleotide; PAR, poly(ADP-ribose); SBDD, structure based drug design; NI site, nicotinamide-ribose binding site; AD site, adenine-ribose binding site.
* Corresponding author at present address: Astellas Pharmaceutical Co. Ltd., 21 Miyukigaoka, Tsukuba 305-8585, Japan. Tel.: +81 29 863 7179; fax: +81 29 852 2971; e-mail: kouji.hattori@jp.astellas.com

0968-0896/$ - see front matter © 2005 Elsevier Ltd. All rights reserved.
doi:10.1016/j.bmc.2005.09.061

in embryonic fibroblasts derived from PARP-1-deficient mice.[3,4] Of the PARP family currently identified, PARP-2 bears the strongest resemblance to PARP-1 and might be functionally similar. PARP-2 binds to DNA and is activated by DNAse-treated DNA. It appears that PARP-2 contributes to the residual PARP activity observed in PARP-1 (−/−) cells after treatment with DNA-damaging agents, suggesting a biological role for PARP-2 in response to DNA damage. Interestingly, the DNA-binding domain of PARP-2 is distinct from PARP-1 and PARP-2 lacks the central automodification domain. The mouse PARP-2, mPARP-2, lacks the zinc-finger-motif, despite DNA-binding activity.

In view of the significant structural information, the first crystal structure available was that of the catalytic domain of chicken PARP-1, which informed us to identify the topology of the donor and acceptor sites harboring the substrate NAD^+ and the ADP-ribose moiety of the poly(ADP-ribose) chain of the target protein, respectively. Furthermore, it helped us to elucidate inhibitor–enzyme interactions for a number of chemically different compounds that showed competition to NAD^+ in its binding fold for the binding mode of inhibitors to the NAD^+-binding site.[5] Recently, the second crystal structure of murine PARP-2 has been solved. Pearl and colleagues have disclosed the catalytic fragment of murine PARP-2, at 2.8 Å resolution, and compared this to the catalytic fragment of PARP-1, with an emphasis on providing a possible framework for rational drug design to develop isoform-specific inhibitors.[6] Furthermore, it has been reported that the PARP catalytic domain shows the highest degree of homology between different species,[7,8] suggesting that PARP inhibitors may have no species-difference in terms of inhibitory activity among human, rat, and mouse PARPs.[9]

Over the last two decades, a large number of PARP-1 inhibitors have been developed,[10] the majority of which mimic to some degree the nicotinamide moiety of NAD^+ and bind to the donor site of the protein. However, the residues in the donor site of PARP-1 that provide hydrogen-bonding interactions with these inhibitors are completely conserved in PARP-2, suggesting that these existing PARP-1 inhibitors would not discriminate between PARP-1 and PARP-2.[6] Furthermore, biological assay data and SAR study on specific PARP inhibitors are rare, thus, the discovery of new PARP-isoform selective ligands presents an exciting challenge and new opportunities to the field.

We have recently discovered some classes of quinazolinones, quinazolidinones, and quinoxalines as potent PARP-1 inhibitors which can represent attractive therapeutic candidates for neurodegenerative disorders such as cerebral ischemia or Parkinson's disease in Figure 1[11]. In this paper, we describe our research on PARP-1 and PARP-2 selective inhibitors using the SBDD analysis by a combination of X-ray analysis and homology modeling.

2. Chemistry

Our initial procedure to prepare quinazolinone analogues linked via appropriate substitution is outlined in Scheme 1. Solid-phase synthesis with Rink amide resin produced rapidly and efficiently the desired quinazolinone derivatives on a 10 mg scale in five steps. Loading commercially available anthranilic acid derivatives onto the support-bound secondary amine employing DIC resulted in amide bond formation. Amide compounds on the resins were subsequently treated with 4-bromobutyryl chloride, followed by N-alkylation with several substituted amines to give the cycloamine derivatives. After cleavage from the resin with a mixture of TFA and CH_2Cl_2 (1:1), treatment with 1 N NaOH gave the desired quinazolinone derivatives in a total yield of 40–80%. Re-synthesis and **1f** were performed using liquid synthesis and in a similar method instead of using resin.

Synthesis of the quinazolidinone derivatives linked with corresponding substitution is outlined in Scheme 2. Treatment of **4** with 4-phenyl-tetrahydropyridine under basic conditions leads to the corresponding ester **5**. Hydrolysis of ester **5** with KOH, which was converted to the corresponding amide by DIC and aq NH_3, followed by KOH under reflux resulted in formation of the desired quinazolidinone ring **2a** and **2b**.

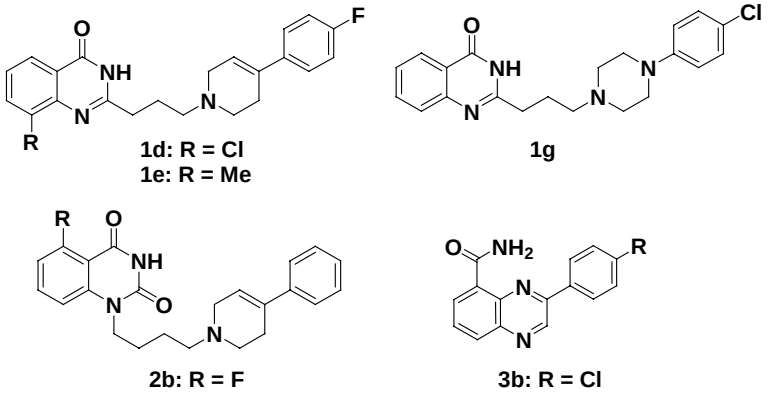

Figure 1.

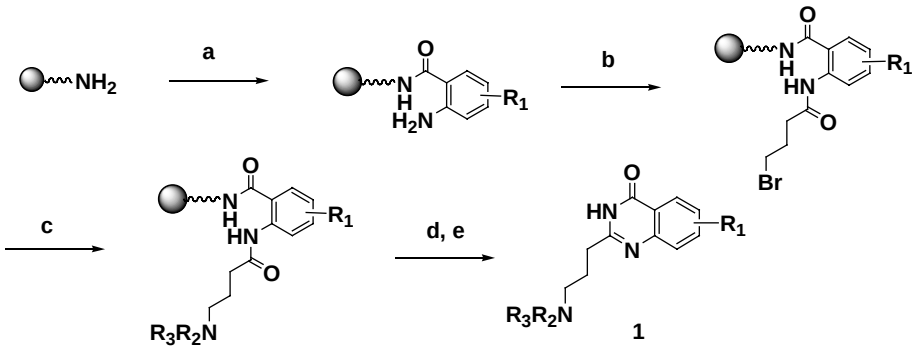

Scheme 1. Reagents: (a) anthranilic acid derivatives, DIC, DMF; (b) 4-bromobutyryl chloride diisopropylethylamine, CH_2Cl_2; (c) 1,2,3,6-tetrahydro-4-phenylpyridine derivatives HCl, diisopropylethylamine, NMP; (d) TFA, CH_2Cl_2; (e) 1 N NaOH, dioxane.

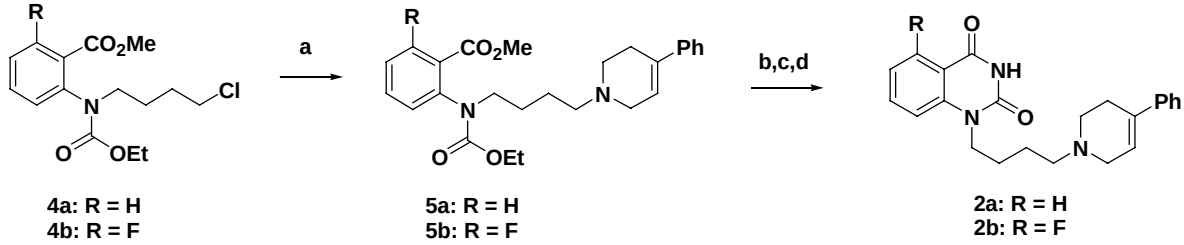

Scheme 2. Reagents: (a) 1,2,3,6-tetrahydro-4-phenylpyridine HCl, K_2CO_3, NaI, DMF; (b) KOH, H_2O–MeOH; (c) DlC, HOBT, THF, then NH_3 aq; (d) KOH, EtOH.

Synthesis of the phthalazinone derivatives is outlined in Scheme 3. Wittig reaction of 4-benzyloxybutanal **6** and phosphonium bromide **7** with triethylamine at room temperature, followed by hydrazine monohydrate, gave the desired phthalazinone ring **8**. Treatment of **8** with BBr_3 gives the corresponding bromide, followed

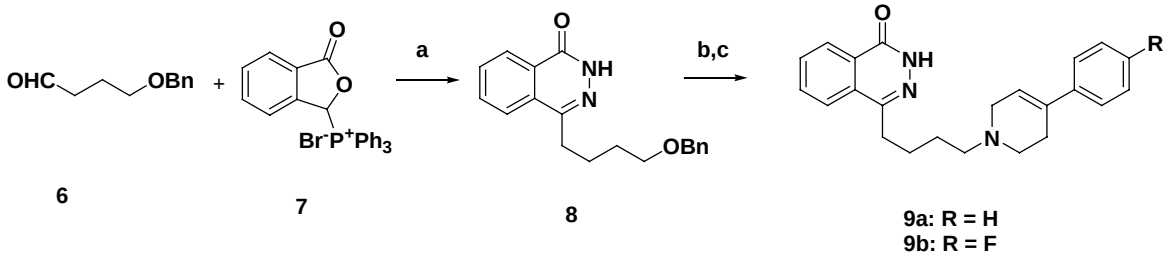

Scheme 3. Reagents: (a) Et_3N, THF, then hydrazine monohydrate, EtOH; (b) BBr_3, CH_2Cl_2; (c) 1,2,3,6-tetrahydro-4-phenylpyridine derivatives HCl, Et_3N, DMF.

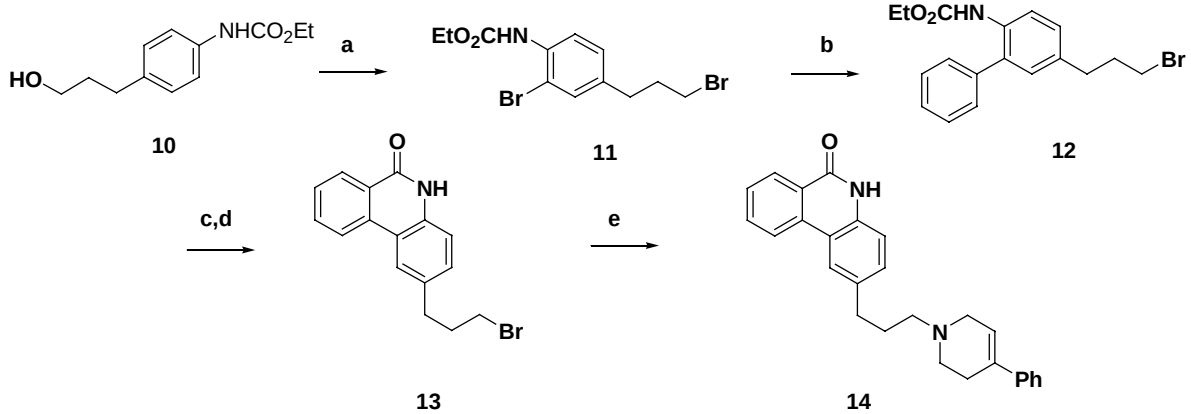

Scheme 4. Reagents: (a) Br_2, AcONa, AcOH; (b) phenylboronic acid, $Pd(PPh_3)_4$, 2 M Na_2CO_3, DME; (c) P_2O_5, $POCl_3$; (d) 4 N HCl, EtOH; (e) 1,2,3,6-tetrahydro-4-phenylpyridine HCl, Et_3N, DMF.

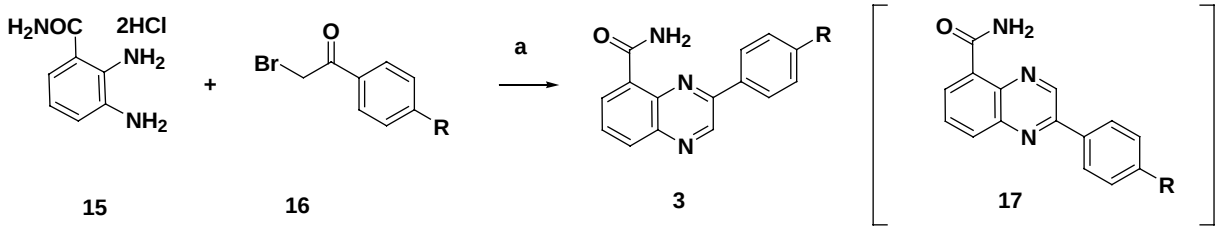

Scheme 5. Reagents: (a) Et_3N, MeOH.

by reaction with the corresponding pyridine derivatives to obtain phthalazinone derivatives **9a** and **9b**.

Synthesis of the phenanthridinone **14** is outlined in Scheme 4. Bromination of the commercially available carbonate **10** with bromine and sodium acetate in acetic acid at the room temperature gives dibromide **11**. After Suzuki coupling with phenylboric acid and $Pd(PPh_3)_4$, diphenyl derivative **12** was treated with P_2O_5 in phosphorus oxychloride at the room temperature, followed by 4 N HCl solution under reflux for 30 min to form the phenanthridinone ring **13**. **13** was treated with the same amine to give the corresponding phenanthridinone **14**.

Finally, synthesis of the quinoxaline derivatives is outlined in Scheme 5. Treatment of 2,3-diaminobenzamide dihydrochloride **15** with the corresponding phenacyl bromide derivatives **16** in the presence of the triethylamine at the room temperature overnight produced a mixture of **3** and minor regioisomer **17**. The mixture was easily purified by column chromatography to give desired quinoxaline derivatives **3**.

3. Results and discussion

3.1. Quinazolinone structure

PARP-1/2 inhibitory activity of quinazolinone derivatives[12] in vitro is outlined in Table 1.[13] In general, the inhibitory potency of these derivatives was found to be largely dependent on the unique linker of the quinazolinone ring. Quinazolinone linked with a 4-phenyl-tetrahyropyridine moiety (**1a**) exhibited strong potency against PARP-1 (IC_{50}: 21 nM) and exhibited appropriately 30-fold less potency against PARP-2 (IC_{50}: 608 nM). The addition of a chloro group at the 8-position (**1b**), which is important for bioavailability and brain penetration, resulted in almost the same activity and selectivity, as previously reported.[11a] Substitution of the *p*-cyano group at the terminal phenyl ring was the most advantageous, with IC_{50} = 3 nM, but the same selectivity was observed. The addition of a methyl group at the 8-position (**1e**) and a chloro group at the 5-position (**1f**) showed three times lower selectivity than **1a**. *N*-Phenylpiperazine derivative (**1g**) also had good activity (IC_{50}: 11 nM) and selectivity (PARP-2/1: 27). On the other hand, well-known inhibitors such as 2-methyl-4(3*H*)quinazolinone (**18**) and 3-AB were less potent and selective, with PARP-2/1: 0.6 and 0.9, respectively.

We performed X-ray crystallography refined to 3.0 Å of the catalytic domain of human PARP-1 complexed with **1e**, as shown in Figure 2.[8] The results indicated that the quinazolinone part of the inhibitor **1e** tightly binds to the nicotinamide-ribose binding site (NI site) and the 4-phenyl-tetrahydropyridine moiety provides secondary contacts to the adenine-ribose binding site (AD site), resulting in improvement of potency. Figure 2B shows the NI site as a critical binding mode for a common

Table 1. PARP-1/2 inhibitory activities of quinazolinone analogues[13]

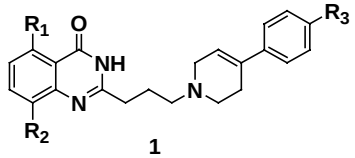

1

Compound	R_1	R_2	R_3	PARP-1 IC_{50} (nM)[a]	PARP-2 IC_{50} (nM)[a]	Selectivity PARP-2/1
1a	H	H	H	21 ± 1.9	608 ± 12.9	29
1b	H	Cl	H	23 ± 1.8	610 ± 18.1	27
1c	H	Cl	CN	3.0 ± 0.6	87 ± 3.6	29
1d	H	Cl	F	13 ± 1.3	500 ± 15.2	39
1e	H	Me	F	16 ± 1.1	167 ± 25.7	10
1f	Cl	H	H	68 ± 2.4	630 ± 28.5	9
1g				11 ± 0.4	300 ± 12	27
18[b]				1200 ± 80	660 ± 24.7	0.6
3-AB[c]				11200 ± 810	9810 ± 770	0.9

[a] The values are presented as means ± SE of three independent experiments (each experiment was triplicate).
[b] 5-Chloro-2-methyl-4(3*H*)-quinazolinone.
[c] 3-Aminobenzamide.

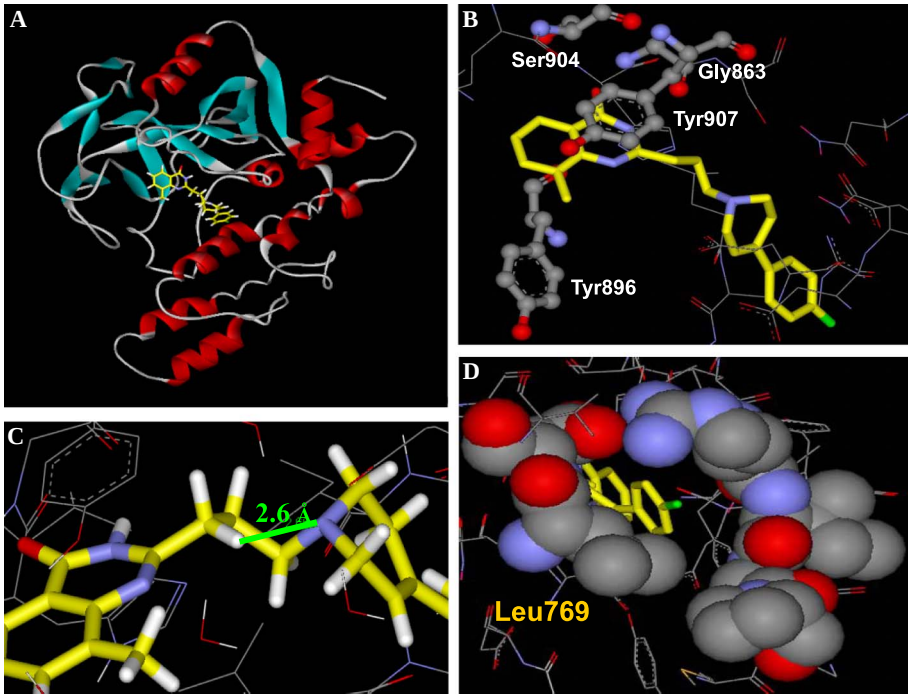

Figure 2. [8,13] (A) X-ray structure (3.0 Å resolution) of compound **1e** in complex with human PARP-1 catalytic domain. **1e** is yellow with heteroatoms being blue for nitrogen, red for oxygen, and green for fluoride. (B) Close-up views of **1e** in the NI site of PARP-1. Important residues in the NI site are shown in ball and stick style. The quinazolinone part was tightly bound by three hydrogen bonds (C═O to Ser904Oγ and Gly863NH, NH to Gly863C═O) and by a sandwiched hydrophobic interaction of Tyr907 and Tyr869. (C) Close-up views of the spacer part of **1e**. Methylene part is twisted and the distance between nitrogen atom and α-CH is 2.6 Å. (D) Close-up views of the terminal site of **1e** in the AD site of PARP-1. The terminal phenyl ring lies in a deep hydrophobic pocket which consists of the side chains of Leu769, Ile879, Pro881, and the methylene chain of Arg878 in PARP-1.

structure motif: three hydrogen bonds (C═O to Ser904-Oγ and Gly863NH, NH to Gly863C═O) and a sandwiched hydrophobic interaction consisting of a π–π interaction with the phenyl ring of Tyr907 and a CH–π interaction with Cβ of Tyr869.[14] 4-Phenyl-tetrahydropyridine moiety of the inhibitor lies in the deep pocket, which consists of the side chains of Leu769, Ile879, Pro881, and the methylene chain of Arg878, by van der Waals interaction in Figure 2D. The spacer part of the inhibitors, which we designed as a three carbon unit to allow a maximum fix of the terminal 4-phenyl-tetrahydropyridine moiety in the AD site, the α-CH_2 is located 2.6 Å from the nitrogen in Figure 2C. As we previously reported, transformation from nitrogen of the pyridine moiety into carbon led to a complete loss of potency of PARP-1[11a] due to the steric hindrance with the α-CH_2 and SP^3 carbon.

Next we performed homology modeling of the catalytic domain of human PARP-2 and **1e** by FAMS[15] based on the solved X-ray structure of murine PARP-2.[6] As expected, there are no differences in the nicotinamide-ribose binding site (NI site) between PARP-1 and PARP-2. The quinazolinone **1e** binds to the NI site of PARP-2 by three hydrogen bonds (C═O to Ser446Oγ and Gly405NH; NH to Gly405C═O) and by a sandwiched hydrophobic interaction with the phenyl ring of Tyr438 and Tyr449 (Fig. 3A). However, the critical difference between PARP-1 and PARP-2 in this hydrophobic pocket in the AD site is the replacement of Leu769 in PARP-1, with Gly314 in PARP-2 (Fig. 3B). Based on these findings, it is clearly suggested that replacement of Leu769 by Gly314 leads to loss of a hydrophobic pocket and leads to a loss of potency against PARP-2. The change of only one amino acid is therefore sufficient to allow discrimination between PARP-1 and PARP-2.

3.2. Quinazolidinone and related structures

Table 2 shows the SAR results of quinazolidinone and related structures. Quinazolidinone structure **2** was discovered from the Fujisawa sample collection and phthalazinone **9** and phenanthridinone **14** have already served as substrates for NAD^+.[16] We designed the related analogues **9** and **14**, which are linked by a unique 4-phenyl-tetrahydropyridine moiety extended with a three- or four-carbon unit by modeling to introduce it to the AD site. In general, these derivatives had similar potency for PARP-1 as the quinazolinone derivatives. However, they did not have selectivity for PARP-1 and PARP-2 in spite of overlapping with the terminal 4-phenyl-tetrahydropyridine moiety of all compounds in AD site. PARP-2/1 selectivities for **2a** and **9a**, and **14** were 1.4 and 0.8, and 1, respectively.

In order to validate our results, we have compared by X-ray crystallography the catalytic domain of human PARP complexes with **2b** and **1e**. Figure 4A shows that quinazolidinone **2b** binds to both the NI and the AD subsites of the donor site in a similar binding mode as **1e**. The quinazolidinone core binds to the NI site by

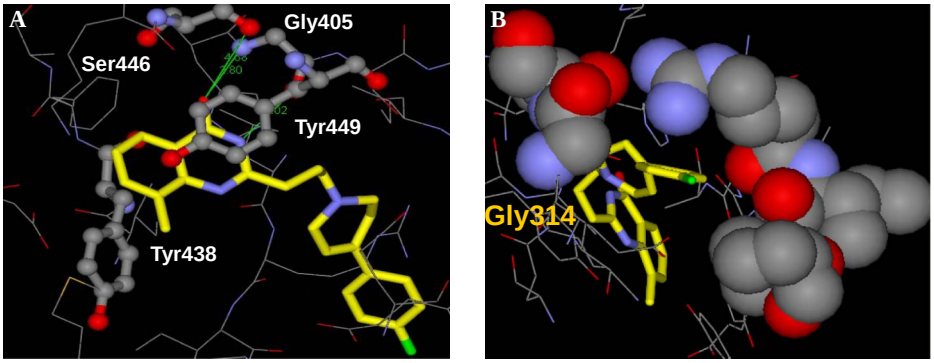

Figure 3. Refs. 13. (A) Homology modeled structure of compound**1e** in complex with human PARP-2 catalytic domain based on the solved X-ray structure (2.8 Å resolution) of murine PARP-2. Important residues in the NI site are shown in ball and stick style. (B) Close-up views of the terminal site of **1e** in the AD site of PARP-2. The replacement of Leu769 in PARP-1with Gly314 in PARP-2.

Table 2. PARP-1/2 inhibitory activities of quinazolidinone and related structures

Compound	R	X	PARP-1 IC_{50} (nM)[a]	PARP-2 IC_{50} (nM)[a]	Selectivity PARP-2/1
2a	H	N	120 ± 3.2	70 ± 3.6	0.6
2b	F	N	60 ± 2.7	83 ± 2.5	1.4
2c	F	C	>1000	NT	
9a	H		120 ± 4.3	90 ± 4.7	0.8
9b	F		49 ± 3.1	84 ± 4.2	1.7
14			82 ± 5.1	84 ± 2.8	1.0

[a] The values are presented as means ± SE of three independent experiments (each experiment was triplicate).

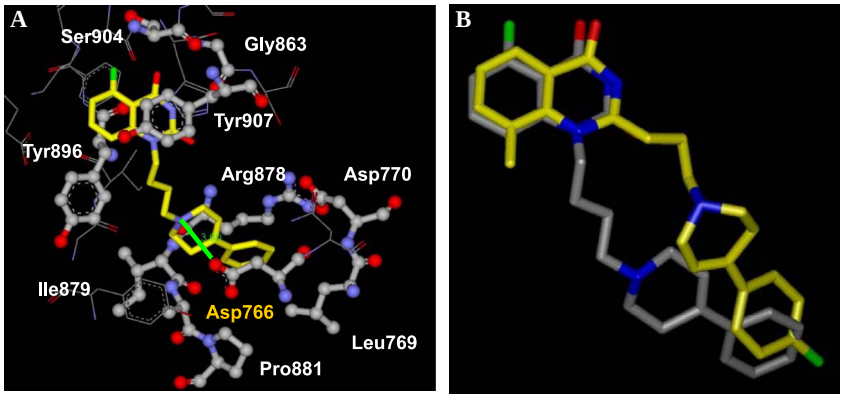

Figure 4. (A) Compound **2b** bound to the human PARP-1 active site. Compound **2b** is yellow with heteroatoms being blue for nitrogen, red for oxygen, and green for fluoride. Important residues are shown in stick style. The nitrogen atom of the terahydropyridine moiety of **2b** directly binds to CO_2H of Asp766 located 3.6 Å from the nitrogen. See Ref. [11a] (B) Overlay of co-crystal structures of **1e** (yellow for carbon) and **2b** (gray for carbon) in the PARP-1 active site.

three hydrogen bonds and by a sandwiched hydrophobic interaction. The terminal phenyl ring lies in the deep pocket by van der Waals interaction in the AD site. The different binding mode is the nitrogen atom of the tetrahydropyridine moiety of **2b**, which directly binds to CO_2H of Asp766 located 3.6 Å from the nitrogen.

Figure 4B displays an overlay of cocrystal structures of **1e** (yellow for carbon) and **2b** (gray for carbon) in the PARP-1 active site, showing that they occupy the same general space in the NI site and AD site. However, the location of the nitrogen atom of the tetrahydropyridine moiety is in a different location. Transformation from nitrogen of pyridine moiety into carbon (**2c**) also led to a complete loss of potency of PARP-1, suggesting that this nitrogen is a very important factor for binding mode between ligand and PARP-1. **2b** and **9**, and **14** overlapped in the same position of the nitrogen atom of 4-phenyltetrahydropyridine by our modeling and show the same potency for PARP-1 and PARP-2. On the other hand, the replacement of Asp766 in PARP-1 with Glu311 in PARP-2 would be expected to lead to a more strong interaction of the CO_2H of Glu311 with the nitrogen atom of side chain to recover the loss of the hydrophobic pocket in PARP-2.

3.3. Quinoxaline structure

The SAR results for quinoxaline derivatives are outlined in Table 3[13]. The activity of these inhibitors against PARP-2 is about 10-fold more potent than against PARP-1. Substitution at the *para* position of the terminal phenyl ring was more advantageous to activity than either *meta* or *ortho* substitution (data not shown). A 2-fold improvement in activity against PARP-2 was obtained by *p*-chloro (**3b**) with $IC_{50} = 7.0$ nM and selectivity: 0.21. Addition of *p*-cyano also gave good potency for PARP-2 ($IC_{50} = 8$ nM) and good selectivity (selectivity: >10-fold).

To validate our results, we performed structural analysis by X-ray crystallography of human PARP-1 complexes with quinoxaline ligand and molecular modeling of PARP-2[13]. Figure 5A shows the structure of the human catalytic domain of PARP-1 complex with **3b**, refined to 3.0 Å. The binding mode of **3b** with human PARP-1 is almost the same as those of the previously disclosed benzimidazole analogues.[17] The carboxamide part of the inhibitor tightly binds to the same NI site by the three critical hydrogen bonds with Ser904 and Gly863, and the nitrogen of the quinoxaline ring binds to the carboxylic acid of Glu988, suggesting that this binding mode was conserved in PARP-2 (Fig. 5B). However, the main differences in the binding site of the terminal phenyl group of quinoxaline analogues within the groove could be used to introduce discrimination between PARP-1 and PARP-2. The Cl-phenyl group of **3b** provides secondary contacts to the side chain of Asp766 formed by a hydrogen bond with Tyr889, which replaces the hydrogen bond between Glu311 and Tyr431 in PARP-2. The second source of selectivity results from the replacement of Glu763 in PARP-1 with Gln308 in PARP-2. X-ray analysis shows that the side chain of Glu763 in PARP-1 is restricted by a hydrogen bond with neighbor Gln759 and Ala760 (Fig. 5A),[18] while the residue of Gln308 in PARP-2 is mobile and can make a more favorable interaction with the Cl-phenyl group, since the previous study indicated that the side chain of Gln763 in chicken PARP-1 appeared to be mobile and movement of this residue nicely accommodated the *p*-benzylamine substitution of inhibitors.[17,19] It is considered that the Cl-phenyl group extends into this groove containing Glu311 and Gln308 in PARP-2 to make a more favorable interaction and may account for the increase in potency observed (Fig. 5C vs. D).

4. Conclusions

We have discovered the first PARP-1 and PARP-2 selective inhibitors. The quinazolinone derivatives are PARP-1 selective and the quinoxaline derivatives are PARP-2 selective. SBDD study by a combination of X-ray analysis and homology modeling has revealed the distinct binding mode for the discrimination between ligands and PARP-1/2. The information from this study should be useful for the further design of novel and selective PARP inhibitors. It is not known at present how PARP inhibition therapy affects the function of PARP isoforms or how inhibition of these isoforms contributes to possible reduction of the side effects. Compounds **1d** and **1g**, and compounds **3b** were found to have a good pharmacokinetic profile with brain penetration. These inhibitors provide important tools for the development of new conceptual medication for neurode-

Table 3. PARP-1/2 inhibitory activities of quinoxaline analogues[13]

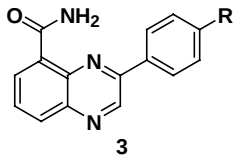

3

Compound	R	PARP-1 IC_{50} (nM)[a]	PARP-2 IC50(nM)[a]	Selectivity PARP-2/1
3a	H	131 ± 2.6	14 ± 1.3	0.11
3b	Cl	33 ± 0.9	7.0 ± 2.0	0.21
3c	CN	101 ± 1.8	8.0 ± 1.0	0.08
3d	CF_3	118 ± 3.1	11 ± 0.9	0.09
3e	OMe	71 ± 2.2	8.0 ± 0.8	0.11
3f	NH_2	87 ± 3.8	9.0 ± 1.0	0.10

[a] The values are presented as means ± SE of three independent experiments (each experiment was triplicate).

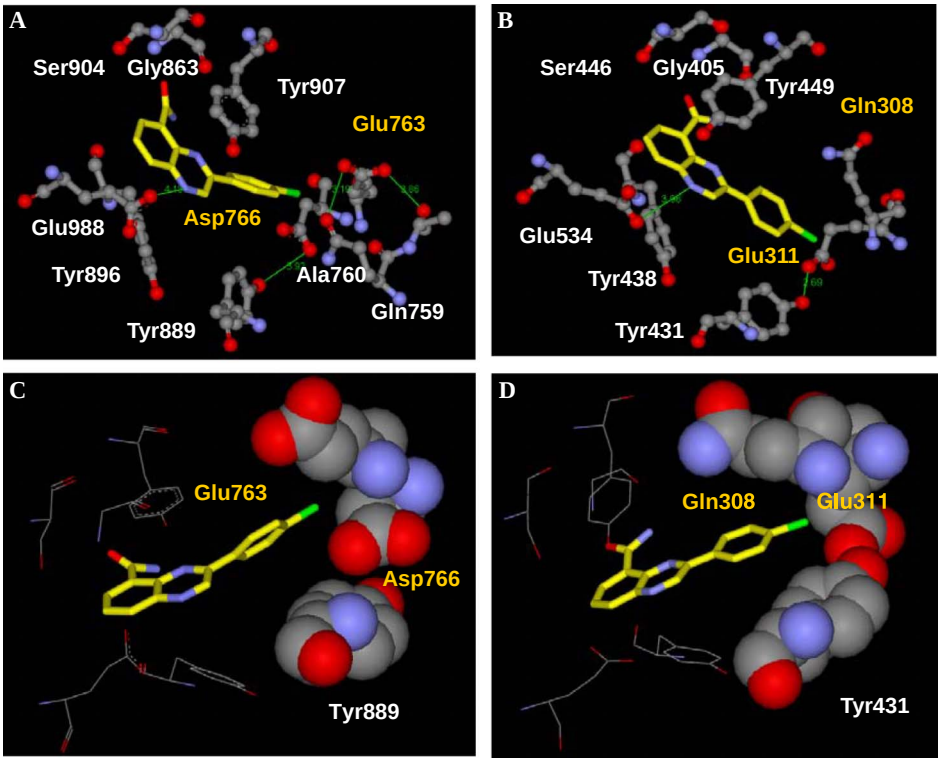

Figure 5. Ref. 13. (A) X-ray structure (3.0 Å resolution) of compound **3b** in complex with human PARP-1 catalytic domain. Compound **3b** is yellow with heteroatoms being blue for nitrogen, red for oxygen, and green for chloride. Important residues in the NI site are shown in ball and stick style. (B) Homology modeled structure of compound**3b** in complex with human PARP-2 catalytic domain based on the solved X-ray structure (2.8 Å resolution) of murine PARP-2. Important residues in the NI site are shown in ball and stick style. (C) Close-up views of the binding mode of the Cl-Phenyl site of **3b** in PARP-1. (D) Close-up views of the binding mode of the Cl-Phenyl site of **3b** in PARP-2.

generative disorders such as cerebral ischemia or Parkinson's diseases.

5. Experimental

5.1. Chemistry

5.1.1. General information. ^{1}H NMR spectra were recorded on a Varian EM-390 NMRspectrometer or a Bruker AC200P spectrometer. Chemical shifts are reported downfield from tetramethylsilane (=0) for ^{1}H NMR. Mass spectra (MS) were determined on a Hitachi Model M-80 mass spectrometer. Elementary analyses were performed on a Perkin-Elmer 2400 CHN elemental analyzer. Reagent and solvent were used as obtained from commercial suppliers without further purification. Chromatographic purification of the compounds was performed on silica gel 60 (63–200 μm) purchased from Merck Co. Recombinant human PARP enzyme was purchased from Trevigen, Inc. (Gaithersburg, MD) and recombinant mouse PARP-1 and PARP-2 enzymes were purchased from Alexis Biochemicals (San Diego, CA).

5.1.2. Solid-phase synthesis of quinazolinone derivatives

1. A solution of anthranilic acid derivatives (5 equiv), pyridine (5 equiv), 1,3-diisopropylcarbodiimide (5 equiv), and DMAP (1 equiv) in DMF (5 mL) was added to a reaction vessel containing Rink amide resin (support-bound secondary amine, 1.0 g, 0.59 mmol/g, loading). After the vessel was shaken for 12 h at ambient temperature, the resin was washed with dichloromethane, and THF, DMF, and dichloromethane.
2. Diisopropylethylamine(10 equiv), 4-bromobutyl chloride (10 equiv), and DMAP (1 equiv) were added to a mixture of the obtained resin in dichloromethane (10 mL). After the vessel was shaken for 12 h at ambient temperature, the resin was washed with dichloromethane, and THF, DMF, and dichloromethane.
3. Cyclic amine derivatives (10 equiv), diisopropylethylamine (10 equiv), and DMAP (1 equiv) were added to a mixture of the obtained resin in *N*-methyl-2-pyrrolidinone (10 mL). After the vessel was shaken for 12 h at ambient temperature, the resin was washed with dichloromethane, and THF, DMF, and dichloromethane.
4. Cleavage from resin was performed with 50% trifluoroacetic acid in dichloromethane (10 mL) for 30 min at ambient temperature. After the filtered solvent was evaporated under pressure, the residue was dissolved in dioxane (5 mL). An aqueous solution of sodium hydroxide (1 M, 5 mL) was added to the solution at room temperature, and the mixture was stirred at that temperature for 15 h. The organic materials were extracted with chloroform, and the organic layer was washed with water and dried over sodium sulfate. Appropriate purification of the crude product by column chromatography on silica gel or HPLC gave the desired product.

5.1.3. Liquid-phase synthesis for quinazolinone derivatives 1a

1. Under a nitrogen atmosphere, a solution of 4-bromobutyryl chloride (4.9 g, 26.4 mmol) in dichloromethane (10 mL) was added dropwise to a solution of 2-aminobenzamide (3.0 g, 22 mmol) in pyridine (18 mL, 220 mmol) and dichloromethane (15 mL) at 0 °C. The mixture was stirred for 1.5 h at 0 °C. The reaction mixture was poured into ice-cooled 1 N hydrochloric acid, and the product was extracted with chloroform. The organic layer was washed with 1 N hydrochloric acid and water, and dried over sodium sulfate. The crude product was triturated with toluene to give 2-[(4-bromobutanoyl)amino]benzamide (5.11 g, 81.3%) as a powder. ^{1}H NMR (200 MHz, $CDCl_3$) δ 2.29 (2H, quint., J = 6.8 Hz), 2.61 (2H, t, J = 7.2 Hz), 3.52 (2H, t, J = 6.4 Hz), 5.5–6.5 (2H, br), 7.09 (1H, dt, J = 7.6, 1.1 Hz), 7.51 (1H, t, J = 7.6 Hz), 7.53 (1H, d, J = 7.6 Hz), 8.62 (1H, d, J = 8.5 Hz), 11.25 (1H, s). API-ESMS: 307 (M^++Na).
2. Under a nitrogen atmosphere, triethylamine (0.73 mL, 5.26 mmol) was added to a solution of 2-[(4-bromobutanoyl)amino]benzamide (500 mg, 1.75 mmol) and 4-phenyl-1,2,3,6-tetrahydropyridine hydrochloride (412 mg, 2.10 mmol) in *N*,*N*-dimethylformamide (5 mL) at 0 °C. The mixture was allowed to warm to room temperature and stirred for 24 h. The reaction was quenched with water, and the product was extracted with chloroform. The organic layer was washed with water and dried over sodium sulfate. Purification over silica gel chromatography gave 2-{[4-(4-phenyl-3,6-dihydro-1(2*H*)-pyridinyl)butanoyl]-amino}benzamide (477 mg, 74.8%) as a pale-yellow powder. ^{1}H NMR (200 MHz, $CDCl_3$) δ 2.01 (2H, quint., J = 7.3 Hz), 2.41–2.56 (4H, m), 2.72 (2H, t, J = 5.4 Hz), 3.76 (2H, d, J = 5.7 Hz), 5.4–6.3 (2H, br), 6.05 (1H, m), 7.05 (1H, t, J = 7.0 Hz), 7.21–7.37 (6H, m), 7.45–7.51 (2H, m), 8.64 (1H, d, J = 8.6 Hz). API-ESMS: 364 (M^++H).
3. 2-{[4-(4-Phenyl-3,6-dihydro-1(2*H*)-pyridinyl)butanoyl]amino}benzamide (475 mg, 1.31 mmol) was dissolved in dioxane (5 mL). An aqueous solution of sodium hydroxide (1 M, 3.92 mL) was added to the solution at room temperature, and the mixture was stirred at that temperature for 15 h. The organic materials were extracted with chloroform, and the organic layer was washed with water and dried over sodium sulfate. Recrystallization of the crude product from chloroform–methanol gave 2-{3-[4-phenyl-3,6-dihydro-1(2*H*)-pyridinyl]propyl}-4(3*H*)-quinazolinone **1a** (329 mg, 72.9%). ^{1}H NMR (200 MHz, CDCl3) δ 2.05 (2H, quint., J = 6.0 Hz), 2.66 (2H, t, J = 6.0 Hz), 2.81–2.94 (4H, m), 3.31 (2H, d, J = 3.2 Hz), 6.12 (1H, t, J = 2.9 Hz), 7.21–7.49 (7H, m), 7.61–7.72 (2H, m), 8.23 (1H, d, J = 6.6 Hz). API-ESMS: 346 (M^++H). Anal. Calcd for $C_{22}H_{23}N_3O$: C, 76.49; H, 6.71; N, 12.16. Found: C, 76.15; H, 6.75; N, 12.12.

5.1.3.1. 8-Chloro-2-{3-[4-phenyl-3,6-dihydro-1(2*H*)-pyridinyl]propyl}-4(3*H*)-quinazolinone (1b): 1b–g were prepared in a similar method. ^{1}H NMR (200 MHz, DMSO-d_6): δ 1.8–2.1 (2H, m), 2.3–2.8 (8H, m), 3.05 (2H, br s), 6.07 (1H, m), 7.2–7.5 (5H, m), 7.86 (1H, dd, J = 8.0, 1.4 Hz), 7.97 (1H, dd, J = 8.0,1.4 Hz). API-ESMS: 380 (M^++H). Anal. Calcd for $C_{22}H_{22}ClN_3O$ + 0.29H_2O: C, 68.61; H, 5.91; N, 10.91. Found: C, 68.60; H, 5.79; N, 10.91.

5.1.3.2. 8-Chloro-2-{3-[4-(4-cyanophenyl)-3,6-dihydro-1(2*H*)-pyridinyl]propyl}-4(3*H*)-quinazolinone (1c). ^{1}H NMR (200 MHz, DMSO-d_6) δ 1.98 (2H, quint., J = 6.9 Hz), 2.3–2.8 (8H, m), 3.11 (2H, d, J = 2.9 Hz), 6.29 (1H, br s), 7.36 (1H, t, J = 7.9 Hz), 7.53(2H, d, J = 8.5 Hz), 7.77 (2H, d, J = 8.4 Hz), 7.90 (1H, d, J = 7.8 Hz), 7.97 (1H, d, J = 7.9 Hz), 12.49 (1H, br). API-ESMS:405 (M^++H). HRMS (EI) 405.1485 [calcd for $C_{23}H_{21}ClN_4$ 405.1482].

5.1.3.3. 8-Chloro-2-{3-[4-(4-fluorophenyl)-3,6-dihydro-1(2*H*)-pyridinyl]propyl} -4(3*H*)-quinazolinone (1d). ^{1}H NMR (200 MHz, DMSO-d_6): δ 1.8–2.1 (2H, m), 2.2–2.8 (8H, m), 3.3 (2H, br s), 6.03 (1H, m), 7.0–7.2 (2H, m), 7.3–7.6 (2H, m), 7.42 (1H, t, J = 8.0 Hz), 7.90 (1H, dd, J = 8.0, 1.4 Hz), 7.99 (1H, dd, J = 8.0, 1.4 Hz). API-ESMS: 398 (M^++H). Anal. Calcd for $C_{22}H_{21}FClN_3O$ + 1.19H_2O: C, 63.02; H, 5.42; N, 10.02. Found: C, 63.01; H, 5.10; N, 9.92.

5.1.3.4. 8-Methyl-2-{3-[4-(4-fluorophenyl)-3,6-dihydro-1(2*H*)-pyridinyl]propyl}- 4(3*H*)- quinazolinone (1e). ^{1}H NMR (200 MHz, DMSO-d_6): δ 1.8–2.0 (2H, m), 2.59 (3*H*, s), 2.4–2.8 (8H, m), 3.0–3.2 (2H, m), 6.05 (1H, m), 7.0–7.5 (5H, m), 7.80 (1H, dd, J = 7.6, 1.4 Hz), 7.95 (1H, dd, J = 7.6, 1.4 Hz). API-ESMS: 378 (M^++H). HRMS (EI) 378.1979 [calcd for $C_{23}H_{25}FN_3O_1$ 378.1982].

5.1.3.5. 5-Chloro-2-{3-[4-phenyl-3,6-dihydro-1(2*H*)-pyridinyl]propyl}-4(3*H*)-quinazolinone (1f). ^{1}H NMR (200 MHz, DMSO-d_6): δ 1.8–2.0 (2H, m), 2.2–2.8 (8H, m), 2.9–3.1 (2H, m), 6.05 (1H, m), 7.1–7.8 (7H, m), 8.01 (1H, d, 1.6 Hz). API-ESMS: 380 (M^++H). Anal. Calcd for $C_{22}H_{22}ClN_3O$: C, 69.56; H, 5.84; N, 11.06. Found: C, 69.54; H, 5.88; N, 11.03.

5.1.3.6. 2-[3-(4-(4-Chlorophenyl)-1-piperazinyl)propyl]-4(3*H*)-quinazolinone (1g). ^{1}H NMR (200 MHz, DMSO-d_6): δ 1.7–2.0 (2H, m), 2.3–2.7 (8H, m), 3.1–3.3 (4H, m), 6.88 (2H, d, J = 9.2 Hz), 7.35 (2H, d, J = 9.2 Hz), 7.38 (1H, t, J = 9.0 Hz), 7.71 (1H, d, J = 9.0 Hz), 7.78 (1H, td, J = 9.0, 1.2 Hz), 8.05 (1H, dd J = 9.0, 1.2 Hz). API-ESMS: 383 (M^++H). Anal. Calcd for $C_{21}H_{23}ClN_4O$ + 1.61 H_2O: C, 61.24; H, 6.42; N, 13.80. Found: C, 61.23; H, 6.22; N, 14.04.

5.1.3.7. Methyl-3-fluoro-2-{(ethoxycarbonyl)[4-(4-phenyl-3,6-dihydro-1(2*H*)-pyridinyl) butyl]amino}benzoate (5b). Sodium iodide (225 mg, 1.50 mmol), potassium carbonate (622 mg, 4.5 mmol), and 4-phenyl-1,2,3,6-tetrahydropyridine hydrochloride (323 mg, 1.65 mmol) were added to a solution of **4b** (543 mg, 1.50 mmol) in *N*,*N*-dimethylformamide (10 mL) at room temperature. The mixture was heated at 80 °C for 3 h. The reaction was quenched by addition of saturated aqueous

ammonium chloride, and the organic materials were extracted with ethyl acetate (647 mg, 89.0%). API-ESMS: 455 (M^++H).

5.1.3.8. 5-Fluoro-1-(4-(4-phenyl-3,6-dihydro-1(2*H*)-pyridinyl)butyl)-2,4(1*H*,3*H*)-quinazolinedione (2b). An aqueous solution of potassium hydroxide (2 M, 5.3 mL) was added to a solution of **5b** (647 mg, 1.33 mmol) in methanol. The mixture was heated at reflux for 14 h. Cooled to room temperature, methanol was removed in vacuo. Neutralized with an aqueous solution of hydrogen chloride, the organic materials were extracted with ethyl acetate. The crude carboxylic acid derivative was used for next step without any purification. *N*,*N*′-diisopropylcarbodiimide (0.418 mL, 2.67 mmol) was added to a solution of carboxylic acid derivative and 1H-1,2,3-benzotriazol-1-ol monohydrate (361 mg, 2.67 mmol) in *N*,*N*-dimethylformamide (10 mL) at room temperature, and the mixture was stirred for 2 h. This mixture was dropped into an excess amount of aqueous solution of ammonia (28%, 8.1 mL), and it was stirred for 1 h at room temperature. The crude product, which the residue was dissolved in ethanol (30 mL). Potassium hydroxide (powder, 180 mg) was added to it, and the mixture was heated at reflux for **2h**. Compound **2b** was obtained by treating the crude product with methanol (165 mg, 30.2%) as a white powder.

^{1}H NMR (200 MHz, DMSO-d_6): δ 1.5–1.8 (4H, m), 2.3–2.7 (6H, m), 3.08 (2H, m), 4.04 (2H, m), 6.17 (1H, br s), 7.00 (1H, dd, J = 8.2, 12.0 Hz), 7.1–7.8 (7H, m). API-ESMS: 394 (M^++H). Anal. Calcd for $C_{23}H_{24}FN_3O + 0.13H_2O$: C, 69.80; H, 6.18; N, 10.62. Found: C, 69.78; H, 6.18; N, 10.54.

5.1.3.9. 1-(4-(4-Phenyl-3,6-dihydro-1(2*H*)-pyridinyl)butyl)-2,4(1*H*,3*H*)-quinazolinedione (2a): Compound 2a was obtained in a similar method as 2b. ^{1}H NMR (200 MHz, DMSO-d_6): δ 1.5–1.8 (4H, m), 2.3–2.7 (6H, m), 3.08 (2H, m), 4.04 (2H, m), 6.20(1H, br s), 7.1–7.5 (7H, m), 7.74 (1H, m), 0.04 (1H, d, J = 8.2 Hz). API-ESMS: 376 (M^++H). Anal. Calcd for $C_{23}H_{25}N_3O_2$-HCl: C, 67.06; H, 6.36; N, 10.20. Found: C, 67.10; H, 6.46; N, 10.11.

5.1.3.10. 5-Fluoro-1-1-[4-(4-phenyl-3-cyclohexen-1-yl)butyl]-2,4(1*H*,3*H*)-quinazolinedione (2c). ^{1}H NMR (200 MHz, DMSO-d_6): δ 1.1–1.7 (8H, m), 1.7–1.9 (2H, m), 2.1–2.5 (3H, m), 4.04 (2H, t, J = 7.3 Hz), 6.12 (1H, br s), 7.03 (1H, dd, J = 11.2, 8.2 Hz), 7.1–7.5 (6H, m), 7.73 (1H, dt, J = 8.4, 6.0 Hz), 11.51 (1H, br s). API-ESMS: 393 (M^++H). HRMS (EI) 393.1975 [calcd for $C_{24}H_{26}FN_2O_2$ 393.1978].

5.1.3.11. 4-[4-(Benzyloxy)butyl]-1(2*H*)-phthalazinone (8). A slurry of 4-benzyloxybutanal, (3-oxo-1,3-dihydro-2-benzofuran-1-yl)(triphenyl)phosphonium bromide (560 mg), and triethylamine (7.39 mL) in tetrahydrofuran (50 mL) was stirred at room temperature overnight. The resulting precipitates were removed by filtration and washed with ethyl acetate, and then the combined filtrate was concentrated. The residue was chromatographed on silica gel using toluene as an eluent to give an oil, which was dissolved in ethanol and refluxed in the presence of hydrazine monohydrate (1.4 g) for 1 h. The mixture was concentrated, then dichloromethane and water were added, and the organic layer was separated. The aqueous layer was further extracted with dichloromethane, then the combined extracts were dried over magnesium sulfate and concentrated. The residue was triturated with dichloromethane and diisopropylether, then the resulting powder was collected, washed with diisopropylether, and dried in vacuo to give the objective compound (2.78 g, 51%).

^{1}H NMR (DMSO-d_6, d): δ 1.50–2.00 (4H, m), 2.94 (2H, t, J = 7.2 Hz), 3.49 (2H, t, J = 6.1 Hz), 4.45 (2H, s), 7.10–7.50 (5H, m), 7.70–8.20 (3H, m), 8.26 (1H, dd, J = 1.9, 7.1 Hz), 12.45 (1H, br s). API-ESMS: 309 (M^++1).

5.1.3.12. 4-{4-[4-(4-Fluorophenyl)-3,6-dihydro-1(2*H*)-pyridinyl]butyl}-1(2*H*)-phthalazinone (9b). To a slurry of 4-[4-(benzyloxy)butyl]-1(2*H*)-phthalazinone in dichloromethane (5 mL) was added dropwise 1 M boron tribromide in dichloromethane (0.97 mL), and the mixture was stirred at room temperature for 2 h. The reaction was quenched with water and extracted with dichloromethane twice. The combined extracts were dried over magnesium sulfate and concentrated. The residue was triturated with diisopropylether, and the resulting powder was collected, washed with diisopropylether, and dried in vacuo. A mixture of 4-(4-Bromobutyl)-1(2*H*)-phthalazinone (100 mg), 4-fluorophenyl-1,2,5,6-tetrahydropyridine hydrochloride (91 mg), and triethylamine (0.149 mL) in *N*,*N*-dimethylformamide (5 mL) was stirred at room temperature overnight. The mixture was diluted with water and extracted with ethyl acetate twice. The combined extracts were washed with water three times, dried over magnesium sulfate, and concentrated. The residue was purified by preparative thin layer chromatography (10% methanol in dichloromethane) to give **9b** (70 mg, 30%) as a colorless powder.

^{1}H NMR (DMSO-d_6): δ 1.40–2.00 (4H, m), 2.30–3.30 (10H, m), 6.12 (1H, s), 7.00–7.60 (5H, m), 7.70–8.00 (2H, m), 8.04 (1H, d, J = 7.6 Hz), 8.26 (1H, d, J = 7.6 Hz), 12.44 (1H, br s). API-ESMS: 378 (M^++1). Anal. Calcd for $C_{23}H_{24}FN_3O + 0.30H_2O$: C, 72.12; H, 6.48; N, 10.98. Found: C, 72.16; H, 6.61; N, 10.77.

5.1.3.13. 4-[4-(4-Phenyl-3,6-dihydro-1(2*H*)-pyridinyl)butyl]-1(2*H*)-phthalazinone (9a). Compound **9a** was obtained by the same method as **9b** ^{1}H NMR (DMSO-d_6): δ 1.10–1.90 (4H, m), 2.30–3.00(8H, m), 3.07 (2H, d, J = 2.8 Hz), 6.15(1H, s), 7.10–8.40 (9H, m), 12.45 (1H, br s). API-ESMS: 360 (M^++1). HRMS (EI) 360.2072 [calcd for $C_{23}H_{26}N_3O_1$ 360.2076].

5.1.3.14. Ethyl 2-bromo-4-(3-hydroxypropyl)phenylcarbamate (11). Bromine (3.51 g) was added to a solution of ethyl 4-(3-hydroxypropyl)phenyl carbamate (**10**) (4.46 g) and sodium acetate (3.28 g) in acetic acid (50 mL). The mixture was stirred for 5 h and the solvent

was evaporated. The residue was diluted with a mixture of water and ethyl acetate and the aqueous layer was separated. The organic layer was washed with saturated aqueous sodium hydrogencarbonate, aqueous sodium thiosulfate, brine, and dried over magnesium sulfate. After evaporation of the solvent, the residue was purified by column chromatography on silica-gel eluting with hexane–ethyl acetate to afford **11** (5.53 g, 92%).

^{1}H NMR (DMSO-d_6): δ 1.32 (3H, t, J = 7.1 Hz), 1.8–2.0 (2H, m), 2.65 (2H, t, J = 7.2 Hz), 3.6–3.7 (2H, m), 4.23 (2H, q, J = 7.1 Hz), 7.02 (1H, br s), 7.13 (1H, dd, J = 8.4, 2.0 Hz), 7.35 (1H, d, J = 2.0 Hz), 8.01 (1H, d, J = 8.4 Hz). API-ESMS: 303 (M^++1).

5.1.3.15. Ethyl 5-(3-bromopropyl)-1,1′-biphenyl-2-ylcarbamate (12). Under a nitrogen atmosphere, phenylboronic acid (437 mg), 2 M aqueous sodium dicarbonate (4.5 mL), tetrakis(triphenylphosphine)palladium (0) (173 mg) were added to a solution of ethyl **11** (1.1 g) in dimethoxyethane (13.5 mL) at room temperature. The mixture was refluxed for 5 h, cooled to room temperature, and poured into a mixture of water and ethyl acetate. The aqueous layer was separated and the organic layer was washed with brine, dried over magnesium sulfate. After evaporation of the solvent, the residue was purified by column chromatography on silica-gel eluting with toluene to afford **13** (1.1 g, 99%).

^{1}H NMR ($CDCl_3$): δ 1.24 (3H, t, J = 7.1 Hz), 2.0–2.4 (2H, m), 2.76 (2H, t, J = 7.0 Hz), 3.40 (2H, t, J = 6.6 Hz), 4.16 (2H, r, J = 7.1 Hz), 6.55 (1H, br s), 7.0–7.5 (7H, m), 8.02 (1H, d, J = 8.3 Hz). Mass 384.1, 386.1 API-ESMS: 384 (M^++Na).

5.1.3.16. 2-(3-Bromopropyl)phenanthridin-6(5*H*)-one (13). Under a nitrogen atmosphere, phosphorus (V) oxide (511 mg) was added to a solution of **12** (435 mg) in phosphorus oxychloride (3 mL) at room temperature. The mixture was refluxed for 2 h and the solvent was evaporated. The residue was poured into a mixture of ice water and ethyl acetate, and the solution was brought to pH 9 with 10% aqueous potassium carbonate. The aqueous layer was separated and the organic layer was washed with brine, dried over magnesium sulfate. The solvent was evaporated in vacuo and the residue was dissolved in a mixture of dioxane (6 mL) and 4 N aqueous hydrogen chloride (3 mL). The solution was refluxed for 30 min, cooled to room temperature, and poured into a mixture of water and ethyl acetate. The mixture was neutralized with 10% aqueous potassium carbonate and the aqueous layer was separated. The organic layer was washed with brine, dried over magnesium sulfate. After evaporation of the solvent, the residue was purified by column chromatography on silica-gel eluting with dichloromethane–acetone to afford **13** (280 mg, 74%).

^{1}H NMR (DMSO-d_6): δ 2.0–2.3 (2H, m), 2.83 (2H, t, J = 7.0 Hz), 3.5–3.7 (2H, m), 7.25–7.4 (2H, m), 7.63 (1H, t, J = 7.1 Hz), 7.85 (1H, dt, J = 7.2, 1.5 Hz), 8.23 (1H, s), 8.32 (1H, dt, J = 7.9, 1.2 Hz), 8.52 (1H, d, J = 8.1 Hz), 11.62 (1H, s). API-ESMS: 316 (M^++1).

5.1.3.17. 2-{3-[4-Phenyl-3,6-dihydropyridin-1(2*H*)-yl]propyl}phenanthridin-6(5H)-one (14). 1,2,3,6-Tetrahydro-4-phenylpyridine hydrochloride (152 mg) was added to a solution of **13** (150 mg) in *N*,*N*-dimethylformamide (3 mL) at room temperature. The mixture was cooled in an ice bath and triethylamine (0.66 mL) was added. The whole mixture was stirred for 1 h with ice cooling and stirred overnight at ambient temperature. The mixture was poured into a mixture of water and ethyl acetate and the aqueous layer was separated. The organic layer was washed with brine and dried over magnesium sulfate. After evaporation of the solvent, the residue was purified by column chromatography on silica gel eluting with dichloromethane–acetone and chloroform–methanol to afford **14** (75 mg, 41%).

^{1}H NMR (DMSO-d_6): δ 1.8–2.0 (2H, m), 2.4–2.5 (4H, m), 2.6–2.8 (4H, m), 3.08 (2H, d, J = 2.8 Hz), 6.15 (1H, s), 7.1–7.5 (7H, m), 7.63 (1H, t, J = 7.2 Hz), 7.84 (1H, t, J = 7.2 Hz), 8.23 (1H, s), 8.32 (1H, d, J = 8.0 Hz), 8.53 (1H, d, J = 8.0 Hz), 11.61 (1H, s). API-ESMS: 395 (M^++1). Anal. Calcd for $C_{27}H_{26}N_2O$ + 0.41H_2O: C, 80.69; H, 6.73; N, 6.97. Found: C, 80.698; H, 6.46; N, 6.88.

5.1.3.18. 3-Phenylquinoxaline-5-carboxyamide (3a). To a suspension of 2,3-diaminobenzamide dihydrochloride (224 mg, 1 mmol) in methanol (10 mL) were added triethylamine (1.4 mL, 10 mmol) and phenacyl bromide (343 mg, 1.5 mmol) at room temperature. The mixture was stirred overnight and poured into a mixture of water and chloroform. The aqueous layer was separated and the organic layer was washed with brine, dried over magnesium sulfate. After evaporation of the solvent, the residue was purified by column chromatography on silica-gel eluting with dichloromethane–acetone to afford **3a** (128 mg, 35%).

^{1}H NMR (200 MHz, DMSO-d_6): δ 7.5–8.2 (8H, m), 9.37 (1H, m), 9.68 (1H, s). API-ESMS: 250 (M^++1). Anal. Calcd for $C_{15}H_{11}N_3O$ + 0.14H_2O: C, 71.55; H, 4.52; N, 16.69. Found: C, 71.56; H, 4.52; N, 16.69.

5.1.3.19. 3-(4-Chlorophenyl)quinxalin-5-carboxyamide (3b). Compounds **3b–f** were prepared in a similar method ^{1}H NMR (200 MHz, DMSO-d_6): δ δ 7.73 (2H, dd, J = 8.6, 2.2 Hz), 7.95–8.00 (2H, m), 8.25–8.45 (4H, m), 9.14 (1H, br s), 9.67 (1H, s). API-ESMS: 284 (M^++1). HRMS (EI) 284.0584 [calcd for $C_{15}H_{11}ClN_3O$ 284.0591].

5.1.3.20. 3-(4-Cyanophenyl)quinoxaline-5-carboxyamide (3c). ^{1}H NMR (200 MHz, DMSO-d_6): δ 7.8–8.6 (7H, m), 9.04 (1H, m), 9.72 (1H, s). API-ESMS: 275 (M^++1). HRMS (EI) 275.0933 [calcd for $C_{16}H_{11}lN_4O$ 275.0937].

5.1.3.21. 3-(4-Trifluoromethylphenyl)quinoxaline-5-carboxyamide (3d). ^{1}H NMR (200 MHz, DMSO-d_6): δ 7.9–8.05 (4H, m), 8.30 (1H, dd, J = 8.3, 1.5 Hz), 8.45–8.60 (3H, m), 8.59 (1H, br s), 9.72 (1H, s). API-ESMS:

340 (M^++1). Anal. Calcd for $C_{16}H_{10}F_3N_3O + 0.54H_2O$: C, 58.77; H, 3.42; N, 12.85. Found: C, 58.76; H, 3.44; N, 12.73.

5.1.3.22. 3-(4-Methoxyphenyl)quinoxaline-5-carboxyamide (3e). ^{1}H NMR (200 MHz, DMSO-d_6): δ 3.87 and 3.88 (total 3H, s), 7.15–7.22 (H, m), 7.85–7.95 (1H, m), 7.98 (1H, br s), 8.23–8.52 (4H, m), 9.44 (1H, br s), 9.63 and 9.64 (total 1H, s). API-ESMS: 280 (M^++1). Anal. Calcd for $C_{16}H_{13}N_3O_2 + 0.04H_2O$: C, 68.63; H, 4.71; N, 15.01. Found: C, 68.61; H, 4.59; N, 14.84.

5.1.3.23. 3-(4-Aminophenyl)quinoxaline-5-carboxyamide (3f). ^{1}H NMR (200 MHz, DMSO-d_6): δ 6.6–6.8 (2H, m), 7.7–8.4 (5H, m), 9.52 (1H, s). API-ESMS: 265 (M^++1). HRMS (EI) 265.1087 [calcd for $C_{15}H_{13}lN_4O$ 265.1089].

5.2. PARP assay

To assess the inhibitory activity of novel inhibitors, the PARP enzyme assay was carried out in a final volume of 100 µl consisting of 50 mM Tris–HCl (pH 8.0), 25 mM $MgCl_2$, 1 mM dithiothreitol, 10 µg activated salmon testes DNA, 0.1 µCi of [adenylate-^{32}P]-NAD, 0.2 units of recombinant human PARP-1, recombinant mouse PARP-1 or PARP-2, and various concentrations of PARP inhibitors. The reaction mixture was incubated at room temperature (23 °C) for 15 min, and the reaction was terminated by adding 200 µl of ice-cold 20% trichloroacetic acid (TCA) and incubated at 4 °C for 10 min. The precipitate was transferred onto GF/B filter (Packard Unifilter-GF/B) and washed three times with 10% TCA solution and 70% ethanol. After the filter was dried, the radioactivity was determined by liquid scintillation counting. IC_{50} values were calculated from the concentration dependence of the inhibition curves by using computer-assisted non-linear regression analyses.

Acknowledgment

We express our thanks to Dr. David Barrett for his critical reading of the manuscript.

References and notes

1. Yu, S. W.; Wang, H.; Poitras, M. F.; Coombs, C.; Bowers, W. J.; Federoff, H. J.; Poirier, G. G.; Dawson, T. M.; Dawson, V. L. Mediation of poly(ADP-ribosepolymerase-1 dependent cell death by apoptosis-inducing factor. *Science* **2002**, *297*, 259–263.
2. Szabo, C.; Dawson, V. L. Role of poly(ADP-ribose)synthetase in inflammation and ischemia–reperfusion. *Trends Pharmacol. Sci.* **1998**, *19*, 287–298.
3. Shieh, W. M.; Ame, J. C.; Wilson, M. V.; Wang, Z. Q.; Koh, D. W. Poly(ADP-ribose)polymerase null mouse cells synthesize ADP-ribose polymerase. *J. Biol. Chem.* **1998**, *273*, 30069–30072.
4. Ame, J. C.; Rolli, V.; Schreiber, V.; Niedergang, C.; Apiou, F.; Decker, P.; Muller, S.; Hoger, T.; Menissier-de Murcia, J.; De Murcia, G. PARP-2, a novel mammalian DNA damage-dependent poly(ADP-ribose)polymerase. *J. Biol. Chem.* **1999**, *274*, 17860–17868.
5. (a) Ruf, A.; Murcia, G.; Schulz, G. E. Inhibitor and NAD^+ binding to poly(ADP-ribose) polymerase as derived from crystal structures and homology modeling. *Biochemistry* **1998**, *37*, 3893–3900; (b) Ruf, A.; Murcia, J. M.; Murcia, G. M.; Schulz, G. E. Structure of the catalytic fragment of poly(ADP-ribose) polymerase from chicken. *Proc. Natl. Acad. Aci. U.S.A.* **1996**, *93*, 7481–7485.
6. Oliver, A. W.; Ame, J. C.; Roe, S. M.; Good, V.; DeMurcia, G.; Pearl, L. H. Crystal structure of the catalytic fragment of murine poly(ADP-ribose)polymerase. *Nucleic Acids Res.* **2004**, *32*, 456–464.
7. De Murcia, G.; Schreiber, V.; Molinate, M.; Saulier, B.; Poch, O.; Masson, M.; Niedergang, C.; Menissier, J. Structure and function of poly(ADP-ribose) polymerase. *Mol. Cell Biochem.* **1994**, *138*, 15–24.
8. Kinoshita, T.; Nakanishi, I.; Warizaya, M.; Iwashita, A.; Kido, Y.; Hattori, K.; Fujii, T. Inhibitor-induced structural change of the active site of human poly(ADP-ribose) polymerase. *FEBS Lett.* **2004**, *556*, 43–46.
9. Iwashita, A.; Yamazaki, S.; Mihara, K.; Hattori, K.; Yamamoto, H.; Ishida, J.; Matsuoka, N.; Mutoh, S. Neuroprotective effects of a novel poly(ADP-ribose)polymerase-1 inhibitor, 2-{3-[4-(4-chlorophenyl)-1-piperazinyl]propyl}-4(3*H*)- quinazolinone (FR255595) in an in vitro model of cell death and in mouse 1-methyl-4-phenyl-1236- tetrahydropyridine model of Parkinson's disease. *J. Pharmacol. Exp. Ther.* **2004**, *309*, 1067–1078.
10. Recent reviews on PARP inhibitors: (a) Peukert, S.; Schwahn, U. New inhibitors of poly(ADP-ribose)polymerase (PARP). *Expert Opin. Ther. Pat.* **2004**, *14*, 1531–1551; (b) Southan, G. J.; Szabó, C. Poly(ADP-ribose)polymerase inhibitors. *Curr. Med. Chem.* **2003**, *10*, 321–340; (c) Cosi, C. New inhibitors of poly(ADP-ribose)polymerase and their potential therapeutic targets. *Expert Opin Ther. Pat.* **2002**, *12*, 1047–1071.
11. (a) Hattori, K.; Kido, Y.; Yamamoto, H.; Ishida, J.; Kamijo, K.; Murano, K.; Ohkubo, M.; Kinoshita, T.; Iwashita, A.; Mihara, K.; Yamazaki, S.; Matsuoka, N.; Teramura, Y.; Miyake, H. Rational approaches to discovery of orally active and brain-penetrable quinazolinone inhibitors of poly(ADP-ribose)polymerase. *J. Med. Chem.* **2004**, *47*, 4151–4154; (b) Iwashita, A.; Mihara, K.; Yamazaki, S.; Matsuura, S.; Ishida, J.; Yamamoto, H.; Hattori, K.; Matsuoka, N.; Mutoh, S. A new poly(ADP-ribose) polymerase inhibitor, FR261529 [2-(4-chlorophenyl)-5-quinoxalinecarboxamide], ameliorates methamphetamine-induced dopaminergic neurotoxicity in mice. *J. Pharmacol. Exp. Ther.* **2004**, *310*, 1114–1124; (c) Iwashita, A.; Tojo, N.; Matsuura, S.; Yamazaki, S.; Kamijo, K.; Ishida, J.; Yamamoto, H.; Hattori, K.; Matsuoka, N.; Mutoh, S. A. novel and potent poly(-ADP-ribose)polymerase-1 inhibitor, FR247304 (5-chloro-2-[3-(4-phenyl-36-dihydro-1(2*H*)-pyridinyl)propyl]-4(3*H*)-quinazolinone attenuates neuronal damage in in vivo and in vivo models of cerebral ischemia. *J. Pharmacol. Exp. Ther.* **2004**, *310*, 425–436(d) Ref. 9.
12. Some quinazolinone-based PARP inhibitors have been identified. (a) Griffin, R. J.; Srinivasan, S.; Bowman, K.; Calvert, A. H.; Curtin, N. J.; Newell, D. R.; Pemberton, L. C.; Golding, B. T. Resistance-modifying agents. 5. Synthesis and biological properties of quinazolinone inhibitors of the DNA repair enzyme poly (ADP-ribose)polymerase (PARP). *J. Med. Chem.* **1998**, *41*, 5247–5256; (b) Banasik, M.; Komura, H.; Shimoyama, M.; Ueda, K. Specific inhibitors of poly(ADP-ribose)synthetase and mono(ADP-ribosyl)transferase. *J. Biol. Chem.* **1992**, *267*, 1569–1575.

13. Iwashita, A.; Hattori, K.; Yamamoto, H.; Ishida, J.; Kido, Y.; Kamijo, K.; Murano, K.; Miyake, H.; Kinoshita, T.; Warizaya, M.; Ohkubo, M.; Matsuoka, N.; Mutoh, S. Discovery of quinazolinone and quinoxaline derivatives as potent and selective poly(ADP-ribose)polymerase-1/2 inhibitors. *FEBS Lett.* **2005**, *579*, 1389–1393.
14. (a) Skalitzky, D. J.; Marakovits, J. T.; Maegley, K. A.; Ekker, A.; Yu, X.-H.; Hostomsky, Z.; Webber, S. E.; Eastman, B. W.; Almassy, R.; Li, J. Tricyclic benzimidazoles as potent poly(ADP-ribose)polymerase-1 inhibitors. *J. Med. Chem.* **2003**, *46*, 210–213; (b) Ferraris, D.; Ficco, R. P.; Dain, D.; Ginski, M.; Lautar, S.; Lee-Wisdom, K.; Liang, S.; Lin, Q.; Lu, M. X.-C.; Morgan, L.; Thomas, B.; Williams, L. R.; Zhang, J.; Zhou, Y.; Kalish, V. J. Design and synthesis of poly(ADP-ribose)polymerase-1 (PARP-1) inhibitors. Part 4: biological evaluation of imidazobenzodiazepines as potent PARP-1 inhibitors for treatment of ischemic injuries. *Bioorg. Med. Chem.* **2003**, *11*, 3695–3707; (c) Costantino, G.; Macchiarulo, A.; Camaioni, E.; Pellicciari, R. Modeling of poly(ADP-ribose)polymerase (PARP) inhibitors. Docking of ligands and quantitative structure–activity relationship analysis. *J. Med. Chem.* **2001**, *44*, 3786–3794.
15. Ogata, K.; Umeyama, H. An automatic homology modeling method consisting of database searches and simulated annealing. *J. Mol. Graphics Mod.* **2000**, *18*, 258–272.
16. Some phthalazin-1(2*H*)-one derivatives and phenanthridinone derivatives, PARP inhibitors have been identified: see in Ref. 10b.
17. (a) Canan Koch, S. S.; Thoresen, L. H.; Tikhe, J. G.; Maegley, K. A.; Almassy, R. J.; Li, J.; Yu, X.-H.; Zook, S. E.; Kumpf, R. A.; Zhang, C.; Boritzki, T. J.; Mansour, R. N.; Zhang, K. E.; Ekker, A.; Calabrese, C. R.; Curtin, N. J.; Kyle, S.; Thomas, H. D.; Wang, L.-Z.; Calvert, A. H.; Golding, B. T.; Griffin, R. J.; Newell, D. R.; Webber, S.; Hostomsky, Z. Novel tricyclic poly(ADP-ribose)polymerase-1 inhibitors with potent anticancer chemopotentiating activity: design synthesis and X-ray cocrystal structure. *J. Med. Chem.* **2002**, *45*, 4961–4974; (b) White, A. W.; Almassy, R.; Calvert, A. H.; Curtin, N. J.; Griffin, R. J.; Hostomsky, Z.; Maegley, K.; Newell, D. R.; Srinivasan, S.; Golding, B. T. Resistance-modifying agents. 9. Synthesis and biological properties of benzimidazole inhibitors of the DNA repair enzyme poly(ADP-ribose) polymerase. *J. Med. Chem.* **2000**, *43*, 4084–4097.
18. In X-ray crystallography of **1e** and **2b**, the side chain of Glu763 in PARP-1 was also restricted by a hydrogen bond with neighbor amino acid.
19. In murine PARP-2, the replacement of Gln308 by Lys308 was observed. The side chain of Lys308 is also not restricted; see Ref. 6.